Analytica Chimica Acta 1374 (2025) 344511

Contents lists available at ScienceDirect

Analytica Chimica Acta

journal homepage: www.elsevier.com/locate/aca

LA-ICP-MS-quantitated boronate affinity magnetic Zr-MOFs prepared via post-modification for glycopeptides enrichment

Feng Zhang [a,1], Sen Zhang [a,1], Xing Liu [b], Wei Gao [a], Jun Luo [b], Yi-fan Pan [a], Wei-Juan Zheng [c], Xin Hu [a], Hong-zhen Lian [a,*]

[a] State Key Laboratory of Analytical Chemistry for Life Science, School of Chemistry & Chemical Engineering and Center of Materials Analysis, Nanjing University, Nanjing, 210023, China
[b] State Key Laboratory of Water Pollution Control and Green Resource Recycling, School of Environment, Nanjing University, Nanjing, 210023, China
[c] State Key Laboratory of Pharmaceutical Biotechnology, School of Life Sciences, Nanjing University, Nanjing, 210023, China

HIGHLIGHTS

- Boronic acid-functionalized magnetic Zr-MOF (mMOF–AAPBA) was synthesized via PDA.
- A protocol to assay B in the nanomaterial was developed by LA-ICP-MS with ICP-OES.
- B matrix reference material was home-prepared for quantitation method validation.
- MMOF–AAPBA capture glycopeptides through synergistic HILIC and BAC mechanisms.
- Saliva and TCMIs were analyzed to confirm the applicability of the nanocomposite.

GRAPHICAL ABSTRACT

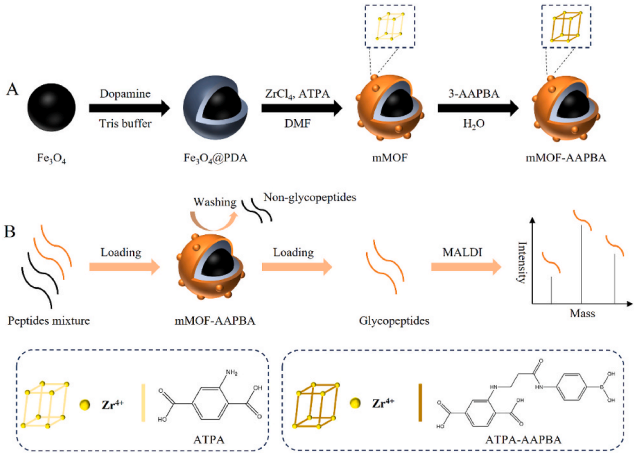

ARTICLE INFO

Handling Editor: Xiu-Ping Yan

Keywords:
Laser ablation inductively coupled plasma mass spectrometry (LA-ICP-MS)
Boron assay
Boronate affinity chromatography (BAC)
Hydrophilic interaction chromatography (HILIC)

ABSTRACT

Background: Glycoproteins are critical in various biological processes and attract lots of attention of researchers. It still remains a challenge to detect glycopeptides by mass spectrometry because of their low abundance with heterogeneity and lability, as well as signal suppression by non-glycopeptides. The boronate affinity-based enrichment is an effective solution for detecting *cis*-diols-containing compounds including glycopeptides in complex matrices. However, there has not been any report about absolute quantitation of boron in the absorbent materials for glycopeptides, which obstructed the tailored design of boronate affinity materials and deeper understanding of interaction mechanisms.
Results: This work presents the development of a boronic acid-functionalized magnetic zirconium metal-organic framework (mMOF–AAPBA) with actual boron content for specific capture of glycopeptides. The synthesized

* Corresponding author.
E-mail address: hzlian@nju.edu.cn (H.-z. Lian).
[1] These authors contributed equally to this work.

https://doi.org/10.1016/j.aca.2025.344511
Received 29 May 2025; Received in revised form 2 August 2025; Accepted 3 August 2025
Available online 5 August 2025

Magnetic solid-phase extraction (MSPE)
Glycopeptide enrichment

nanocomposite could enrich glycopeptides by magnetic solid-phase extraction (MSPE) via the synergistic effect of hydrophilic interaction and boronate affinity. After full characterization including quantitative analysis of boron by laser ablation inductively coupled plasma mass spectrometry (LA-ICP-MS), mMOF–AAPBA was applied as MSPE absorbent to capture glycopeptides. Under the optimized conditions, it could enrich 28 glycopeptides both from horseradish peroxidase and immunoglobulin digests, with a limit of detection of 1 fmol μL^{-1} coupled with matrix-assisted laser desorption/ionization time of flight mass spectrometry. The boronate affinity absorbent also possessed great ability of anti-interference and good reusability. Furthermore, it possessed high performance in enriching glycopeptides in real samples including human saliva and traditional Chinese medicine injections.

Significance: In the preparation of the boron-containing nanocomposites, there is a special interest that an accurate protocol was established to assay boron based on LA-ICP-MS assisted by home-made matrix reference substances for the first time. These findings highlight the quantitative boron-containing mMOF–AAPBA as a robust affinity material for glycopeptide enrichment in real biological samples, offering potential applications in glycoproteomics and other *cis*-diols compound related researches.

1. Introduction

Protein glycosylation, as one of the most diverse post-translational modifications, forms glycoproteins through enzymatic glycosylation. Glycoproteins not only participate in regulating protein folding, stability, and cell signaling [1], but also play a crucial role in aging and diseases [2]. In bottom-up proteomics studies, glycoproteins are first digested, and glycopeptides are then enriched from the resulted peptide mixture for mass spectrometry (MS) detection [3,4]. While MS such as matrix-assisted laser desorption/ionization time of flight mass spectrometry (MALDI-TOF MS) enables high-throughput protein identification, analyzing glycoproteins in complex samples remains a significant challenge. This is because glycopeptides usually constitute a tiny fraction of the total peptide mixture, and their signal intensity is generally lower compared to non-glycopeptides, often being suppressed by the presence of non-glycopeptides [5–7]. Therefore, in glycoproteomics research, it is crucial to preprocess samples to separate and enrich glycopeptides, enhancing the detection sensitivity and analytical efficiency of glycoproteins to better understand their functions and mechanisms in organisms.

To date, various strategies have been developed for the selective enrichment of glycoproteins/glycopeptides, including hydrophilic interaction chromatography (HILIC) [8], boronate affinity chromatography (BAC) [9], lectin affinity [10], and hydrazine chemistry [11]. Among these enrichment strategies, HILIC and BAC are the most common ones for magnetic solid-phase extraction (MSPE) separation.

The selective enrichment mechanism of HILIC involves separating glycopeptides of stronger hydrophilicity from non-glycoproteins and non-glycopeptides with weaker hydrophilicity, using their different retention behaviors in a hydrophilic stationary phase and a hydrophobic organic mobile phase. Hydrophilicity can be introduced by modifying the surface with various substances such as polydopamine (PDA) [12], metal-organic framework materials (MOFs) [13], covalent organic framework materials (COFs) [14], tryptophan [15], glutathione [16], and so on. Among them, PDA, derived from dopamine, stands out in diverse natural hydrophilic compounds including chitosan [17], phytic acid [18], carrageenan [19], sodium alginate [20], and the like. It could become an ideal hydrophilic modifier for magnetic nanoparticles in MSPE to enhance the performance of glycoprotein/glycopeptide enrichment strategies, for its biocompatibility, ease of modification, and ability to mimic the adhesive properties of natural adhesives. Besides, it meets the demands of green chemistry, which emphasizes sustainability, eco-friendliness, the use of renewable resources, the incorporation of green chemical substances into the design of materials, and encourages the development of innovative materials that minimize the use of toxic organic reagents and reduce environmental impact. MOFs, with the advantages of low density, high porosity and large surface area, have garnered considerable attention. In the great family of MOFs, Zr-based MOFs, with a metal center of Zr, have some special characteristics, such as the uniform adjustable structure, great chemical stability brought by strong Zr–O bonds and large coordination numbers, convenience of chemical modification, and incomparable biocompatibility, making them appropriate materials to modify the surface of nanoparticles [21,22].

Boronate affinity relies on the reversible binding of boronic acid groups with *cis*-diols under different pH conditions to accomplish enrichment of target analytes with *cis*-diol structures [23]. The reversible binding of boronic acid and *cis*-diols offers unique advantages in solid-phase extraction. The formation and dissociation of cyclic esters, controlled by pH, enable easy manipulation of the adsorption/elution process. Besides, boronate affinity materials are valued for their broad-spectrum affinity and high specificity to *cis*-diols-containing compounds, as well as easy pH-based control and rapid desorption kinetics, making them increasingly popular in recent years. In the past decades, the need for proteomics and glycomics researches has driven the rapid development of boronate affinity materials. New types, including nanomaterials [14,24,25], molecularly imprinted polymers [26], mesoporous materials [27], and monoliths [28], have been developed to separate various *cis*-diol compounds like glycoproteins [24,25], carbohydrates [29], nucleotides [30], and glycolipids [31].

In these past studies [24–31], the qualification of boron in the synthesized materials mainly depends on infrared spectrometry (IR), X-ray photoelectron spectrometry (XPS) and energy dispersive X-ray spectrometry (EDS). However, the absolute quantification of boron has merely been reported, hindering the specific design of materials and the strict deduction of reaction mechanisms. The major method is XPS to relatively quantify boron in previous boronate affinity solid-phase extraction materials [32–34]. Due to the fact that XPS can only detect relative elemental content at the materials' surface, it is difficult to achieve accurate quantitative determination of B in boronate affinity nanomaterials. As for EDS, boron has a Kα line of low energy (0.183 keV) and extremely low X-ray yield, and the beryllium window in conventional EDS absorbs most of its signal. Thus, B also can hardly be detected by EDS. Other techniques like universal ICP-MS and ICP-OES heavily rely on the digestion of material samples, suffering from boron loss via volatilization, significantly impairing measurement accuracy. To our knowledge, there is no report on the absolute quantification of boron in boronate affinity nanocomposites so far.

Laser ablation inductively coupled plasma mass spectrometry (LA-ICP-MS) is a powerful analytical technology that enables high sensitive elemental and isotopic analysis to be performed directly on solid samples. It begins with a laser beam focused on the sample surface to generate fine particles. The ablated particles forming an aerosol are then transported to the plasma torch of ICP-MS instrument by helium for atomization and ionization of sample components, which are subsequently introduced to a mass spectrometer detector for both elemental and isotopic analysis.

There are basically two categories of strategies [35,36] when modifying boronic acid on MOFs: (1) post-synthetic modification of boronic acid; (2) introducing boronic-acid-containing ligands during the

synthesis of MOFs. Comparing to the second category, post-modification could expose more binding sites of boronic acid on the surface and has a higher utilization efficiency of reactants.

This present work developed a boronic acid-functionalized magnetic zirconium metal-organic framework material and applied it for separation and enrichment of glycopeptides. After UiO-66–NH_2 was modified on PDA-coated Fe_3O_4 nanoparticles to produce Fe_3O_4@PDA@UiO-66–NH_2 (mMOF), a post-synthetic modification approach was used to introduce boronic acid groups by reacting with 3-acrylamidophenylboronic acid (AAPBA). The obtained mMOF–AAPBA was well characterized. Especially, B and Zr were precisely quantified with a newly proposed LA-ICP-MS-based method. Subsequently, horseradish peroxidase (HRP) digests were used to optimize loading and elution conditions. Under optimal conditions, the detection limit, anti-interference ability, and reusability of mMOF–AAPBA were investigated. The enrichment performance of mMOF–AAPBA was further evaluated on immunoglobulin G (IgG) digests. Finally, the applicability of mMOF–AAPBA was assessed in real samples, including human saliva and traditional Chinese medicine injections (TCMIs). Experimental results demonstrated that mMOF–AAPBA could effectively enrich glycopeptides from both model and real samples, providing an ideal alternative absorbent for MSPE to enrich glycopeptides from complex samples.

2. Experimental section

2.1. Chemicals

Methanol, dimethylformamide (DMF), 3-acrylamidophenylboronic acid (AAPBA), acetonitrile (ACN, HPLC grade) and ammonium bicarbonate (NH_4HCO_3) were bought from Macklin (Shanghai, China). Anhydrous sodium acetate, ethanol, ethylene glycol, H_3PO_4 (85 %) and urea were bought from Sinopharm Chemical Reagent Co. Ltd. (Shanghai, China). $ZrCl_4$, ZrO_2 and trifluoroacetic acid (TFA, HPLC grade) were bought from Aladdin (Shanghai, China). 2-Aminoterephthalic acid (ATPA) and 2,5-dihydroxybenzoic acid (DHB, HPLC grade) were bought from TCI (Shanghai, China). $FeCl_3{\cdot}6H_2O$ and dopamine hydrochloride were bought from Heowns (Shanghai, China). Tris (hydroxymethyl)aminomethane (Tris) were bought from Biofroxx (Einhausen, Germany). Dithiothreitol (DTT) was bought from Roche Diagnostics (Mannheim, Germany). Iodoacetamide (IAA), horseradish peroxidase (HRP), immunoglobulin G (IgG), bovine serum albumin (BSA) and trypsin from bovine pancreas (TPCK treated) were bought from Sigma-Aldrich (St. Louis, MO, USA). All chemicals mentioned above were analytical grade except indicated in brackets and could be used without further purification. Ultrapure water was prepared with a Milli-Q water purification system (Millipore, Billerica, MA, USA). Human saliva samples were provided by healthy volunteers and obtained by standard "drooling method", which was approved by the Medical Ethical Committee of Nanjing University. TCMIs Shenmai (SM), Qingkailing (QKL) and Reduning (RDN) injections were provided by Jiangsu Institute for Food and Drug Control (Nanjing, China).

2.2. Synthesis of mMOF–AAPBA

The synthesis process of mMOF–AAPBA is shown in Scheme 1A. The preparation of Fe_3O_4@PDA@UiO-66–NH_2 (mMOF) based on the previous work of our research group [37] is described in Text S1 in Supporting Information. Subsequently, boronic acid was post-modified on Fe_3O_4@PDA@UiO-66–NH_2 according to Ref. [38] with minor adjustment. In brief, 0.10 g mMOF and 0.08 g AAPBA were carefully added into the bottom of 25 mL polytetrafluoroethylene liner, and 10 mL ultrapure water was added into the liner. After being sonicated for 20 min to make the suspension mixed well, the liner was placed into a stainless-steel high-pressure reaction kettle. The kettle was sealed and maintained at 120 °C for 48 h. After the kettle was cooled, the resulted mMOF–AAPBA nanocomposites were separated with a magnet and then washed three times with ultrapure water and ethanol. Finally, mMOF–AAPBA was dried under vacuum at 50 °C overnight.

2.3. Characterization of mMOF–AAPBA

Transmission electron microscopy (TEM) images were taken on a Tecnai G2 F20S-TWIN microscope (FEI, Hillsboro, OR, USA). Scanning electron microscopy (SEM) images were taken on a S–3400 N II microscope (Hitachi, Tokyo, Japan) connected to a Bruker Quantax 200 energy-dispersive spectrometer (EDS, Bruker, Karlsruhe, German). Fourier-transform infrared (FT-IR) spectra were obtained on a Nicolet-

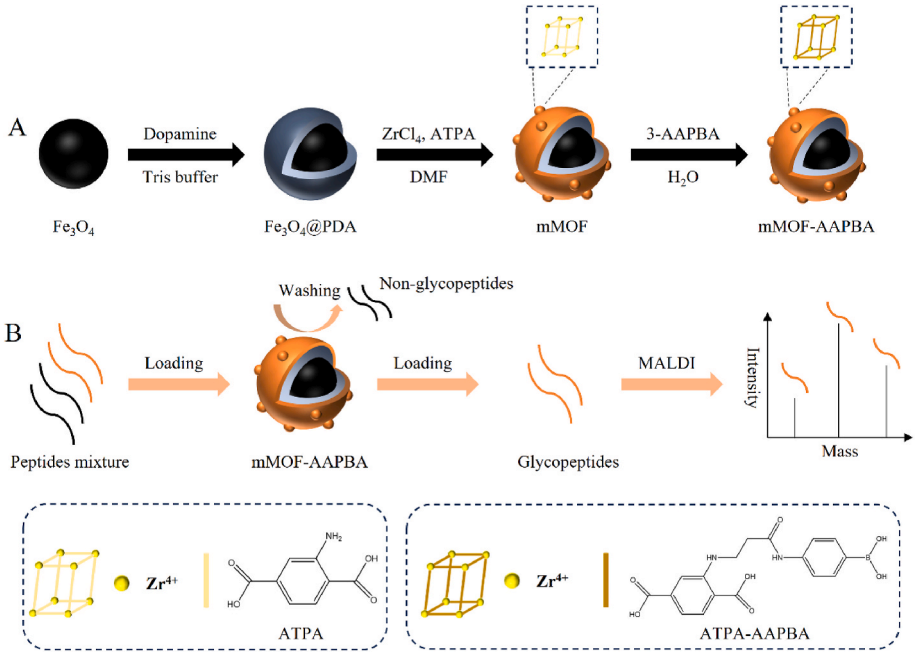

Scheme 1. Synthesis strategy of mMOF–AAPBA (A) and strategy for enrichment of glycopeptides using mMOF–AAPBA as MSPE absorbent (B).

6700 FT-IR spectrometer (Thermo-Fisher, Waltham, MA, USA) in attenuated total reflection (ATR) mode. Thermal analysis was conducted using a STA-499C analyzer (Netzsch, Selb, Germany). Brunauer–Emmett–Teller (BET) surface area analysis was performed on an ASAP 2460 system (Micromeritics, Norcross, GA, USA). X-ray diffraction (XRD) patterns were collected using a Bruker D8 Advance diffractometer (Bruker, Karlsruhe, Germany). X-ray photoelectron spectroscopy (XPS) was performed on a PHI5000 Versa Probe spectrometer (ULVAC Technology, Kanagawa, Japan). The hysteresis loop was measured on a superconducting quantum interference device-vibrating sample magnetometer (SQUID-VSM, Quantum Design, San Diego, CA, USA). The water contact angles of the materials were measured on a KRÜSS DSA30S drop shape analyzer (Hamburg, Germany). LA-ICP-MS analysis was performed on a laser ablation (New Wave, Cambridge, U.K.) coupled with an inductively coupled plasma mass spectrometry (NexION 300, PerkinElmer, Waltham, MA, USA). Inductively coupled plasma optical emission spectroscopy (ICP-OES) was performed on an Avio 500 system (PerkinElmer, Waltham, MA, USA). The adsorption capacity of mMOF–AAPBA towards HRP was analyzed by UV–vis spectrophotometry on a NanoDrop 2000 spectrophotometer (Thermo-Fisher, Waltham, MA, USA).

2.4. Determination of B and Zr

2.4.1. Preparation of home-made matrix reference materials (MRMs)

The matrix reference materials (MRMs) were home-made to accurately quantify B in the mMOF–AAPBA nanocomposites prepared in this work. Determination of an element in the same or similar composition can eliminate the matrix influence on the result. Based on the ingredients of mMOF–AAPBA, Fe_3O_4, ZrO_2, ATPA and AAPBA were chosen as the components of MRMs, where $ZrCl_4$ was replaced with ZrO_2 due to the instability of $ZrCl_4$ in moisture air. The details of MRMs are listed in Table 1, in which, m_{Fe3O4}, m_{ZrO2}, m_{ATPA} and m_{AAPBA} are the weighed amounts of Fe_3O_4, ZrO_2, ATPA and AAPBA for preparing MRMs respectively, and m_{Total} is their total weighed amount, while wt_B and wt_{Zr} are the final weight percentage contents of B and Zr in MRMs respectively.

2.4.2. Determination of B and Zr by LA-ICP-MS

The laser system of LA-ICP-MS, with wavelength quadrupled to 213 nm, was equipped with a large format ablation cell. Line scans of the sample pellets were carried out at a spot size of 100 μm, a scanning speed of 100 μm s^{-1}, an interline spacing of 400 μm, a repetition rate of 20 Hz, and an energy output of 0.012 J cm^{-2}. ^{13}C was used as the internal standard to correct variations in ablation, transport, and ionization efficiency. Signals of B and Zr were recorded for the quantitative determination of them in the sample assayed. The LA system focuses a laser beam on the sample surface, instantly vaporizing small sample particles, which forms an aerosol that is transported to ICP system by helium. Therefore, for powdered samples, it is necessary to compress them into pellets to prevent dispersal by helium into the ablation chamber [39]. The mMOF–AAPBA pellets were pressed using a tablet press shown in Fig. 1. Before sent to LA-ICP-MS analysis, the pressed pellets were fixed onto glass slides with double-sided adhesive tape.

2.4.3. Determination of Zr by ICP-OES

In order to accurately determine B content in mMOF–AAPBA by LA-ICP-MS, Zr content determined in the nanocomposite by ICP-OES was used as internal standard. 0.1 g of mMOF–AAPBA was accurately weighed and placed in a PTFE beaker. Then 5 mL of concentrated HNO_3 and 0.5 mL of H_2O_2 were added and allowed to sit for several hours and be heated on a hot plate. After cooling, 0.5 mL of H_2O_2 was added and heated until nearly dry, and then a small amount of concentrated HNO_3 and H_2O_2 were added multiple times until the solution is clear. The solution was concentrated to 2 mL to remove excess HNO_3 and H_2O_2, and transferred to a 25 mL volumetric flask for dilution to volume with ultrapure water for ICP-OES determination of Zr concentration. Parameters of ICP-OES are given in Table S1.

2.5. Sample preparation of standard glycoproteins and actual samples

Tryptic digestion of HRP, IgG and BSA was carried out following our previous work [37]. Text S2 in Supporting Information provided the procedures in detail. The pretreatment of human saliva involved mixing the saliva with 2 % TFA at a volume ratio of 1:1. The mixture was incubated at 25 °C for 1 h, followed by centrifugation. The supernatant was then collected and centrifugally concentrated by a Labconco CentriVap Vacuum Concentrator (Labconco, Kansas City, MO, USA) to remove the solvent. As for TCMIs, the tryptic digestion method for HRP-spiked SM injection solution is as follows: 87 μL of 1.0 mg mL^{-1} HRP solution was added to 10 mL of SM injection to prepare the HRP-spiked SM injection solution. The 10 mL HRP-spiked SM injection solution was ultrafiltered using an Ultra-15 centrifugal filter unit (Millipore, Billerica, MA, USA). After the membrane was washed three times with 100 mM NH_4HCO_3, the proteins retained on the membrane were redissolved in approximately 1 mL of 100 mM NH_4HCO_3. The following digestion steps were consistent with the method for IgG. The obtained solutions were then centrifugally concentrated to remove the solvent. The tryptic digestion procedures and spiking levels for QKL injection and RDN injection were consistent with those used for SM injection. All the sample solutions mentioned above were stored at −20 °C before use.

2.6. Enrichment of glycopeptides and MALDI-TOF MS analysis

The work process of glycopeptides enrichment is also shown in Scheme 1B. Before enrichment, HRP or IgG digests was diluted to desired concentration, and human saliva and the injection remnants were redissolved into 1.0 mL of 90 % ACN - 9.9 % H_2O - 0.1 % TFA (volume ratio) solution. And then, an aliquot of 10 μL mMOF–AAPBA dispersion (20 mg mL^{-1}) was added to 200 μL of the sample solution. Subsequently, the mixture was vortexed at room temperature for 45 min. The mMOF–AAPBA was separated with the assistance of a magnet. After being washed with loading solution, 10 μL of 30 % ACN - 69 % H_2O - 1 % TFA taken as the eluent was added to elute the adsorbed glycopeptides by vortexing. The supernatant was collected and detected by MALDI-TOF MS described as follows.

After glycopeptides enrichment with mMOF–AAPBA, 1.0 μL of the collected supernatant was spotted onto target spots of MALDI-TOF MS target plate using a pipette gun. After evaporation of the added supernatant, 1.0 μL of DHB matrix (20 mg mL^{-1} dissolved in 50 % ACN - 49 %

Table 1
Information of MRMs.

MRMs	m_{Fe3O4}	m_{ZrO2}	m_{ATPA}	m_{AAPBA}	m_{Total}	wt_B	wt_{Zr}	wt_B/wt_{Zr}
	g					%		
Std.S_2.0	0.1110	0.0670	0.0322	0.0692	0.2794	1.8096	17.7544	0.1019
Std.S_1.0	0.1177	0.0710	0.0677	0.0356	0.2920	0.8908	18.0095	0.0495
Std.S_0.5	0.1177	0.0710	0.0854	0.0180	0.2921	0.4502	18.0033	0.0250
Std.S_0.2	0.1177	0.0710	0.0954	0.0074	0.2915	0.1855	18.0403	0.0103
Std.S_0.1	0.1177	0.0710	0.0982	0.0032	0.2901	0.0806	18.1274	0.0045

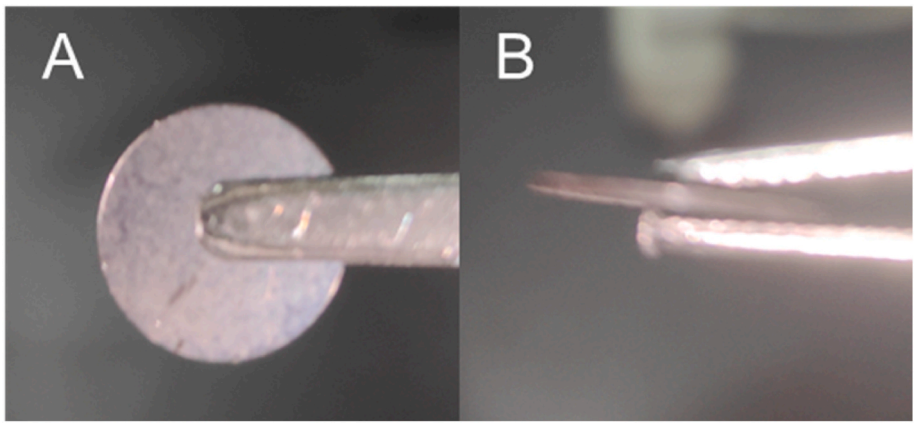

Fig. 1. Digital image of mMOF-AAPBA pellet in front view (A) and side view (B).

H_2O - 1 % H_3PO_4) was spotted onto the target spots. The dried sample spots were analyzed using a Bruker ultrafleXtreme MALDI-TOF/TOF mass spectrometer (Bruker, Karlsruhe, Germany). The analysis employed Smartbeam-II laser in positive reflection mode, with an acceleration voltage of 25 kV.

3. Results and discussion

3.1. Characterization of mMOF–AAPBA

The morphology of mMOF–AAPBA was characterized by TEM and SEM. TEM images at different magnifications of mMOF–AAPBA (Fig. 2A–C) revealed nanoparticles with a distinct core-shell structure and a well-defined spherical shape. SEM images at different magnifications of mMOF–AAPBA (Fig. 2D–G) showed numerous protrusions on the surface of the nanoparticles, which was probably caused by modification with UiO-66–NH_2. Additionally, the spherical structure of the nanoparticles was well-preserved after modification of UiO-66–NH_2. The EDS elemental mapping images corresponding to Fig. 2G (Fig. 2H–K) clearly demonstrated that the Fe, Zr, N, and O elements were evenly distributed in mMOF–AAPBA.

FT-IR spectra of the prepared Fe_3O_4@PDA, mMOF, and mMOF–AAPBA are shown in Fig. 3A. The FT-IR spectrum of Fe_3O_4@PDA shows peaks at 1606 and 1505 cm^{-1} corresponding to the stretching vibration of aromatic C═C bonds, a peak at 1437 cm^{-1} corresponding to the bending vibration of N–H bonds, and a peak at 1294

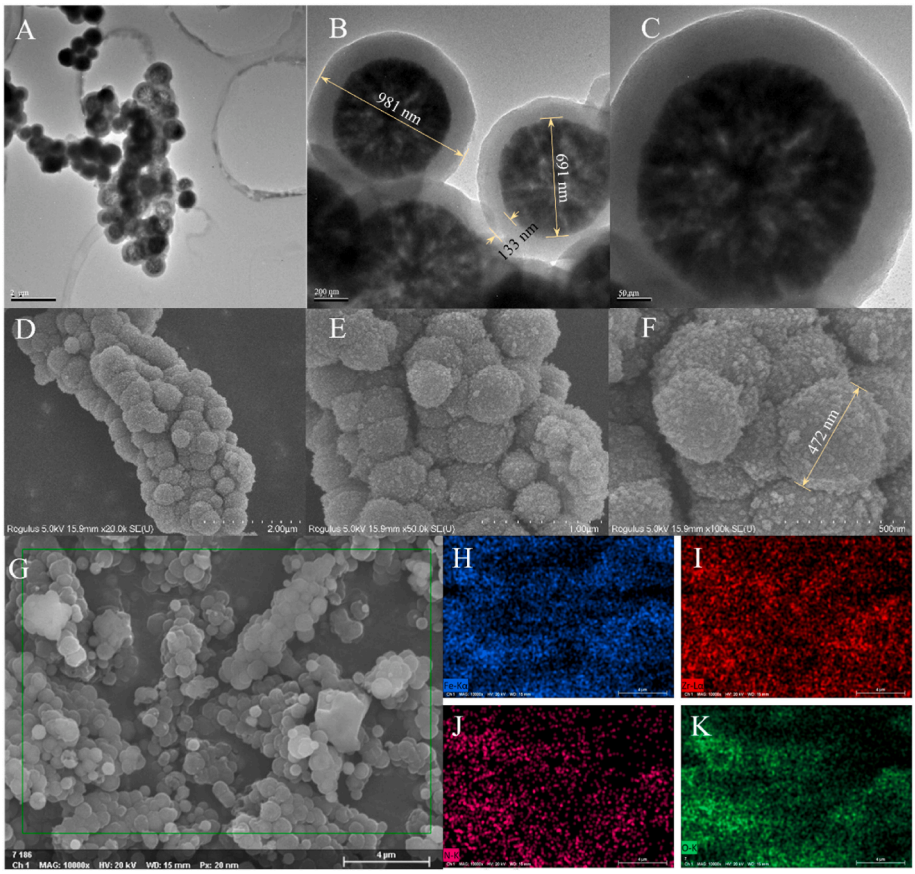

Fig. 2. TEM images of mMOF–AAPBA (A–C); SEM images (D–G) and SEM-EDS elemental mapping pictures of G: Fe (H), Zr (I), N (J), O (K).

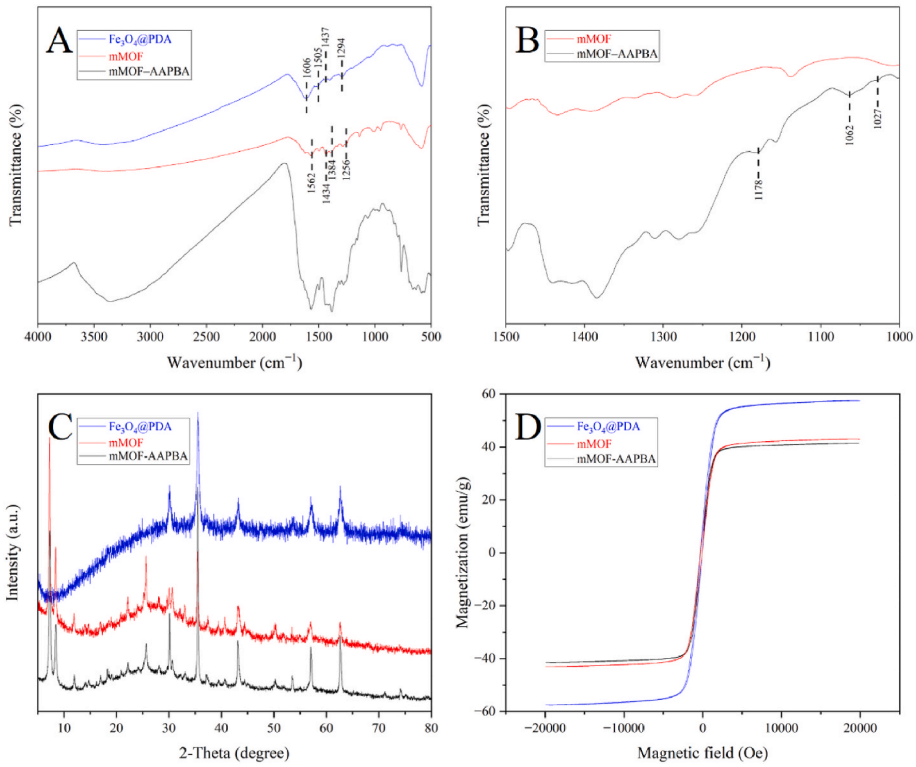

Fig. 3. FT-IR spectra of Fe_3O_4@PDA, mMOF and mMOF–AAPBA (A); FT-IR spectra of mMOF and mMOF–AAPBA between 1500 and 1000 cm^{-1} (B); XRD patterns of Fe_3O_4@PDA, mMOF and mMOF–AAPBA (C); Magnetization curves of Fe_3O_4@PDA, mMOF and mMOF–AAPBA (D).

cm^{-1} corresponding to the stretching vibration of C–O bonds. The FT-IR spectrum of mMOF exhibits enhanced peaks at 1384 and 1434 cm^{-1} attributed to the symmetric stretching vibrations of the carboxyl groups, and a new peak at 1562 cm^{-1} assigned to the asymmetric stretching vibrations of the carboxyl groups in the amino-terephthalic acid ligand of Zr-MOF. The peak at 1256 cm^{-1} corresponded to the stretching vibration of the C–N bonds in ATPA and PDA. Upon modification with AAPBA, the intensities of peaks between 1500 and 1000 cm^{-1} increased. Fig. 3B showed an enlarged view of the spectra of mMOF and mMOF–AAPBA in this region, where new absorption peaks appeared at

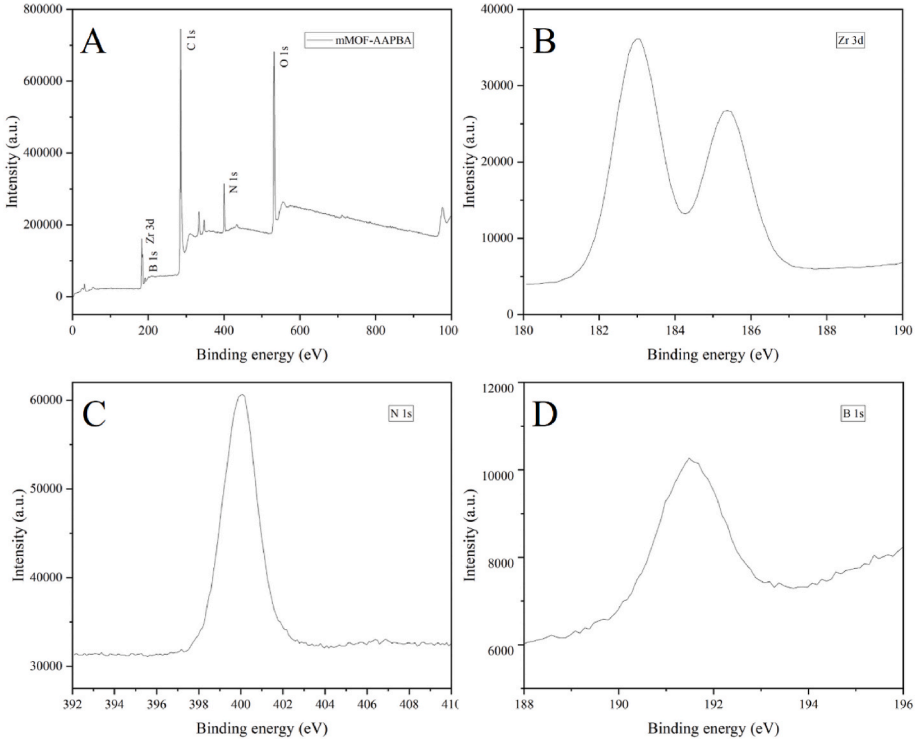

Fig. 4. XPS full scan spectrum of mMOF–AAPBA (A); Zr 3d (B), N 1s (C) and B 1s (D) XPS segmented spectra of mMOF–AAPBA.

1178, 1062, and 1027 cm^{-1}. According to the literature [35], these peaks were respectively attributed to the bending vibration of the B–O bonds, stretching vibration of the C–B bonds, and bending vibration of the B–O bonds, reflecting the modification with boronic acid groups. Fig. 3C presented the XRD patterns of Fe_3O_4@PDA, mMOF and mMOF–AAPBA. All three XRD patterns exhibit strong diffraction peaks at 2θ values of 30.2°, 35.5°, 43.2°, 53.5°, 57.1°, and 62.7°, respectively corresponding to the (220), (311), (400), (422), (511), and (440) crystal planes of Fe_3O_4. Compared to Fe_3O_4@PDA, new strong diffraction peaks appeared at 2θ values of 7.4° and 8.5° in the XRD patterns of mMOF and mMOF–AAPBA, which were characteristic peaks of UiO-66–NH_2, respectively indicating the synthesis of MOF and the retention of structure after boronic acid modification. To characterize the magnetic response of mMOF–AAPBA to an external magnetic field, a vibrating sample magnetometer was used to test the magnetism of Fe_3O_4@PDA, mMOF, and mMOF–AAPBA. The resulting hysteresis curves were shown in Fig. 3D. Upon modification with AAPBA, the saturation magnetization of mMOF–AAPBA was 41.5 emu•g^{-1}, obviously lower than Fe_3O_4@PDA but slightly lower than mMOF, because AAPBA modification only involves reaction with ATPA causing no significant mass increase. The high magnetic response means that the nanomaterial can be rapidly separated from a solid-liquid mixture in a magnetic field.

XPS was then used to determine the elemental composition of mMOF–AAPBA. As shown in Fig. 4, the XPS spectrum of mMOF–AAPBA clearly displays peaks for B 1s, C 1s, N 1s, O 1s, and Zr 3d, indicating the presence of Zr-MOF and boronic acid groups. Since XPS typically analyzes a thin layer of about 10 nm from the surface [40], and Fe_3O_4 was coated with PDA, Fe element could not be detected. The XPS results listed in Table S2 showed an atomic percentage (at%) of 2.42 % for B and 1.73 % for Zr, while a weight percentage (wt%) of 1.83 for B and 11.01 for Zr. Fig. S1 shows the SEM-EDS spectrum of mMOF–AAPBA. Due to the deeper scanning depth of EDS, more of the inner Zr atoms and Fe atoms are detectable, resulting in an increased atomic percentage of Zr (2.92 %) compared to XPS, and an evident signal for Fe that was not observed by XPS. However, due to the limitations of the EDS detection principle [41], B could not be detected by this technique yet.

To investigate the hydrophilicity of the materials, water contact angles were measured. As shown in Fig. S2, the water contact angles of Fe_3O_4, Fe_3O_4@PDA, mMOF and mMOF–AAPBA were 37.7°, 35.1°, 18.8° and 24.0°, respectively. According to the results, after the coating of PDA and modification of MOF, the hydrophilicity of the prepared materials increased. And after the modification of AAPBA, the hydrophilicity slightly decreased because AAPBA is less hydrophilic than mMOF and thus decrease the hydrophilicity of mMOF–AAPBA. Even though, mMOF–AAPBA possessed great hydrophilicity. Together with the introduction of boronate groups, mMOF–AAPBA was able to enrich glycopeptides through the synergetic effects of HILIC and BAC.

To assess the adsorption capacity of mMOF–AAPBA as a MSPE adsorbent, its specific surface area was measured via N_2 adsorption/desorption using BET analysis. The isotherm (Fig. S3) shows a type IV curve, with a BET surface area of 44.48 $m^2\ g^{-1}$ and a total pore volume of 0.058 $cm^3\ g^{-1}$, indicating good adsorption capacity. Then, the adsorption capacity of mMOF–AAPBA was investigated using HRP as a model substance. As shown in Fig. S4, its adsorption capacity to HRP was 15.2 mg g^{-1}.

Thermal stability test (Fig. S5) reveals a 5 % weight loss from room temperature to 100 °C due to water and solvent evaporation, followed by another 5 % loss up to 275 °C from dehydroxylation. Between 275 °C and 600 °C, a 52 % weight loss occurs due to MOF decomposition and PDA carbonization.

3.2. Determination of B in mMOF–AAPBA

As the performance of boronate affinity greatly depends on the proportion of boronic acid ligands in mMOF–AAPBA, a new method was established for accurate assay of boron in the materials through LA-ICP-MS validated via home-made MRMs in combination with ICP-OES in this work. After reaction to synthesize mMOF–AAPBA, the actual amount remained unknown of each element in mMOF–AAPBA, including zirconium, although the ingredient dose was known. Therefore, series MRMs consisting of Fe_3O_4, ZrO_2, ATPA and AAPBA were made in the lab to simulate the components of mMOF–AAPBA. Because zirconium is stable and not easy to be introduced by non-human factors, it was chosen as the internal standard to quantify boron. The MRMs of gradient content and three times of mMOF–AAPBA were tested using LA-ICP-MS, and the signal intensities of B and Zr (SI_B and SI_{Zr}) were recorded in Table S3 and Table 2, respectively for MRMs and mMOF–AAPBA. The LA-ICP-MS spectra of MRMs (Std.S_1.0 in Table 1) and mMOF–AAPBA are depicted in Fig. S6. Based on the actual ingredient weights (Table 1) and the signal intensities (Table S3) of MRMs, a linear relationship (Fig. S6A) between the signal intensity ratio of B to Zr (SI_B/SI_{Zr}) and the weight ratio of B to Zr (wt_B/wt_{Zr}) could be established with a correlative coefficient (R^2) of 0.9991:

$$\frac{SI_B}{SI_{Zr}} = 0.3657 \times \frac{wt_B}{wt_{Zr}} - 0.0005$$

Subsequently, wt_B/wt_{Zr} of mMOF–AAPBA was calculated based on the equation, as well as the SI_B and SI_{Zr} values from Fig. S6B. With the signal intensity recorded from LA-ICP-MS and the average Zr content in the prepared mMOF–AAPBA determined by ICP-OES (wt_{Zr} = 12.62 %), its B weight content (wt_B) is finally calculated as listed in Table 2. The average weight content of B of triplicate in the mMOF-AAPBA was (0.482 ± 0.038)%, with relative standard deviations (RSD) of 7.8 %. The result obtained from the proposed protocol is much smaller than XPS result (B weight percentage of 1.83 %, Table S2), mainly because XPS can't deeply see through the nanocomposite, causing a higher value of the amounts of the elements on the surface of the material.

3.3. Performance of glycopeptide enrichment by mMOF–AAPBA

Prior to evaluating the glycopeptide enrichment performance of mMOF–AAPBA with model protein digests, the loading and elution conditions were optimized for glycopeptide enrichment. For loading, mixtures of ACN/H_2O/TFA with varying acetonitrile ratios (95 % ACN - 4.9 % H_2O - 0.1 % TFA, 90 % ACN - 9.9 % H_2O - 0.1 % TFA, and 85 % ACN - 14.9 % H_2O - 0.1 % TFA) were investigated, as reported in previous studies [36]. The 90 % ACN mixture provided the best results (Fig. S7), increasing glycopeptide peaks while reducing non-glycopeptide peaks. Therefore, 90 % ACN - 9.9 % H_2O - 0.1 % TFA was selected for subsequent experiments. For elution, ACN ratio was fixed at 30 % to check the effect from the concentration of TFA (2 %, 1 %, and 0.5 %). And ACN ratio was tested (20 %, 30 %, and 40 %) with a fixed TFA concentration of 1 %. As indicated by the data in Figs. S8 and S9, the optimal elution condition was 30 % ACN - 69 % H_2O - 1 % TFA, as it effectively eluted glycopeptides while minimizing non-glycopeptide peaks.

Fig. 5A shows the mass spectrum of a 100 fmol μL^{-1} HRP tryptic digest without any enrichment, where non-glycopeptide peaks dominate the spectrum. The high concentration of non-glycopeptides leads to a strong matrix effect, which suppresses the signals from low-abundance glycopeptides. However, after enrichment with mMOF–AAPBA (Figs. 5B), 28 distinct glycopeptide peaks were identified, indicating successful glycopeptide isolation. Detailed information about these enriched glycopeptides is provided in Table S4. To assess the sensitivity of mMOF–AAPBA for detecting glycopeptides, it was applied to HRP tryptic digests at lower concentrations of 10 and 1 fmol μL^{-1} (Fig. 5C and D). Notably, even at 1 fmol μL^{-1}, 5 glycopeptide peaks could still be detected, underscoring the material's ability to enrich low-abundance glycopeptides effectively. Similarly, enrichment of IgG tryptic digests also demonstrated strong performance (Fig. 6). After treatment with mMOF–AAPBA, 28 glycopeptide peaks were observed at a concentration of 100 fmol μL^{-1} (Fig. 6B), with detailed data listed in Table S5. Even at

Table 2
LA-ICP-MS detection results of mMOF–AAPBA (n = 3).

Times	SI_B	SI_{Zr}	SI_B/SI_{Zr}	wt_B/wt_{Zr}	wt_B/%	Mean/%	RSD/%
1	901388	59411605	0.01517	0.04162	0.525	0.482	7.8
2	895972	68058777	0.01317	0.03613	0.456		
3	2443725	181942076	0.01343	0.03686	0.465		

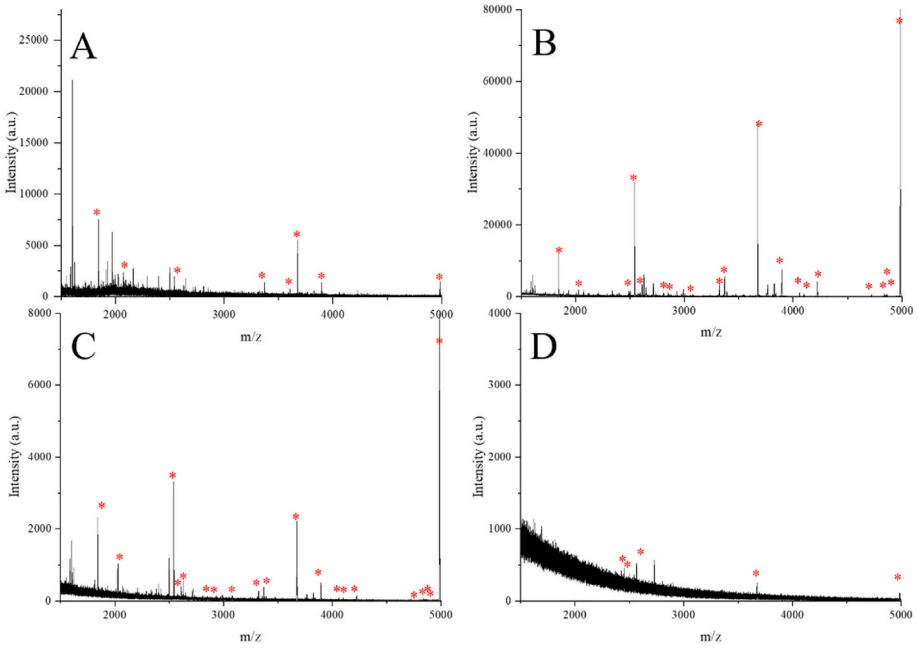

Fig. 5. MALDI-TOF mass spectrum of 100 fmol μL^{-1} HRP tryptic digests before mMOF–AAPBA enrichment (A) and MALDI-TOF mass spectra of HRP tryptic digests after enrichment with mMOF–AAPBA at different concentrations of 100 fmol μL^{-1} (B), 10 fmol μL^{-1} (C) and 1 fmol μL^{-1} (D). Peaks of glycopeptides are labeled with "*".

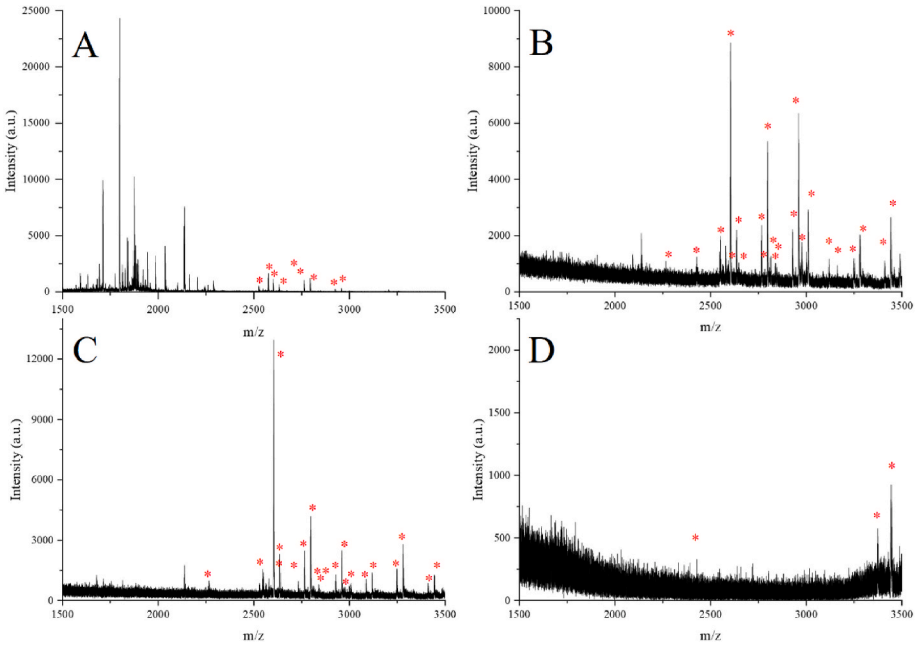

Fig. 6. MALDI-TOF mass spectrum of 100 fmol μL^{-1} IgG tryptic digests before mMOF–AAPBA enrichment (A) and MALDI-TOF mass spectra of IgG tryptic digests after enrichment with mMOF–AAPBA at different concentrations of 100 fmol μL^{-1} (B), 10 fmol μL^{-1} (C) and 1 fmol μL^{-1} (D). Peaks of glycopeptides are labeled with "*".

the lower concentration of 1 fmol μL^{-1}, 5 glycopeptide peaks remained visible, further illustrating the low detection limit of the method (Fig. 6D). The enhanced detection sensitivity can be attributed to the combined effects of HILIC and BAC. The hydrophilicity is provided by the abundant amino and hydroxyl groups in PDA, the Zr–O clusters in Zr-MOF, and the amide groups introduced via boronic acid modification. The affinity for glycopeptides is enhanced by the boronic acid groups, while the integrated Fe_3O_4 nanocore endows the material with robust magnetic responsiveness. This enables a streamlined, gentle magnetic separation process that significantly reduces sample manipulation and minimizes solvent consumption compared to traditional centrifugation/filtration methods.

In real application, glycopeptides face interference not only from non-glycopeptides derived from glycoproteins but also from other proteins and various non-protein substances. To evaluate the interference resistance and selectivity of mMOF–AAPBA, it is critical to assess its ability to enrich glycopeptides in the presence of high concentrations of peptides derived from non-glycosylated proteins. By preparing mixtures of HRP and BSA digests at molar ratios of 1:20, 1:50, and 1:100, and then using mMOF–AAPBA for glycopeptide enrichment, the results are depicted in Fig. 7. Remarkably, even at an HRP-to-BSA molar ratio of 1:100, 14 glycopeptide peaks of high intensity were detected post-enrichment, with the mass spectrum predominantly showing glycopeptides and minimal interference from non-glycopeptides present in the BSA digest. This indicates that mMOF–AAPBA exhibits strong selectivity for glycopeptides, even in complex mixtures. The high selectivity is primarily attributed to the strong hydrophilicity contributed by amide groups, Zr-MOF and polydopamine, as well as the specific affinity from the boronic acid groups, which provides excellent recognition of glycopeptides through HILIC and BAC mechanisms, enabling efficient isolation of glycopeptides from complex biological matrices.

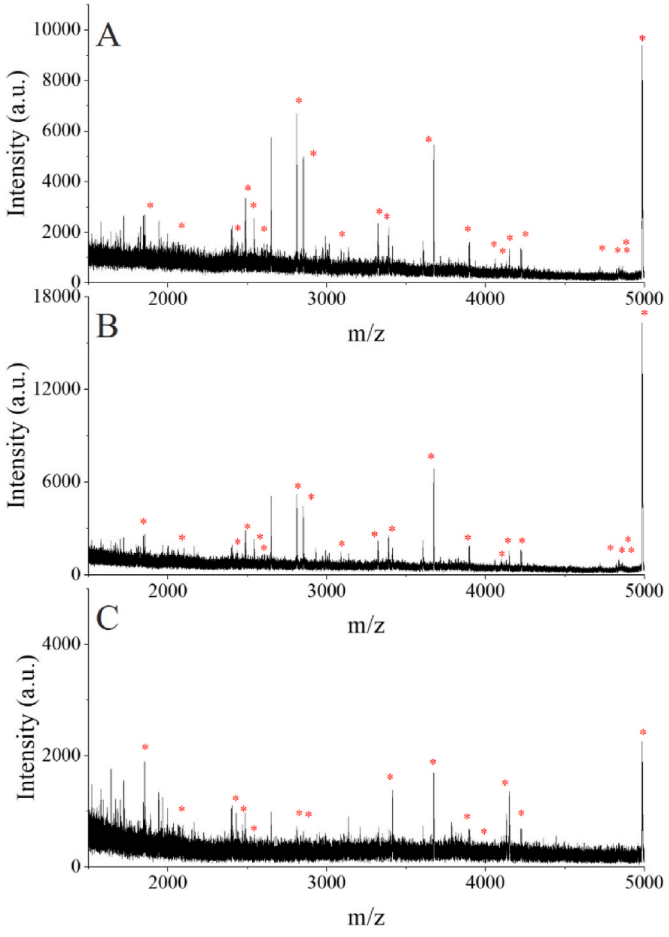

Fig. 7. MALDI-TOF mass spectra of HRP and BSA tryptic digests mixture enriched with mMOF–AAPBA at different molar ratios of 1:20 (A), 1:50 (B) and 1:100 (C). Peaks of glycopeptides are labeled with "*".

Key performance indicators for MSPE materials include their reusability and whether their enrichment efficiency declines after repeated use. To assess the reusability of mMOF–AAPBA, glycopeptide enrichment was performed over multiple cycles using the same batch of the material. After each cycle, the mMOF–AAPBA was thoroughly washed with elution solution and equilibrated with loading solution before the next round of enrichment. As shown in Fig. S10, mMOF–AAPBA enriched 21, 20, and 20 glycopeptide peaks across three consecutive uses. These results demonstrate that mMOF–AAPBA maintains its enrichment capability after multiple uses, highlighting its strong reusability and chemical stability in glycopeptide enrichment.

3.4. Application of mMOF–AAPBA in real complex samples

Research on enrichment and detection of low-abundance glycopeptides in saliva has become a hotspot because these molecules can serve as non-invasive biomarkers for early disease diagnosis and monitoring. Since saliva is a complex sample containing other biochemical molecules, it is necessary to perform separation and enrichment of low-abundance endogenous glycopeptides before detection [42,43]. As shown in Fig. 8A, before enrichment, only three very weak glycopeptide peaks were identified from human saliva. After enrichment with mMOF–AAPBA, 24 glycopeptide peaks were observed, as compared with the published literatures (Fig. 8B) [15,16,44]. The mass spectrum peaks were predominantly glycopeptide peaks, demonstrating the applicability of mMOF–AAPBA for glycopeptide enrichment in actual samples. Detailed information about the glycopeptides enriched from human saliva by mMOF–AAPBA is shown in Table S6.

The increasing concerns about the safety of Traditional Chinese Medicine injections (TCMIs) have highlighted the importance of precise and reliable detection methods, particularly for proteins and other biomolecules that may be present in low abundance. Even in low abundance, proteins might cause severe adverse drug reaction such as hypersensitivity. These concerns have driven the need for more sensitive and accurate analytical techniques with separation and enrichment strategies to ensure the safety and efficacy of TCMIs [45,46]. Mass spectra of glycopeptide enrichment using mMOF–AAPBA in human saliva demonstrate the material's capability to enrich glycopeptides in biological fluids. Three kinds of TCMIs, SM, QKL and RDN injections were further investigated. As shown in Fig. 8C, the direct detection of HRP-spiked SM injection showed numerous high-intensity peaks from polysorbate 80 which was used as a solubilizer and stabilizer in TCMIs, severely suppressing signals of glycopeptides, with only two low-intensity glycopeptide peaks observed. After enrichment with mMOF–AAPBA (Figs. 8D), 21 glycopeptide peaks were observed, and the signals of the interfering peaks were greatly decreased. The enrichment results of HRP-spiked QKL injection and RDN injection are shown in Fig. S11 and S12, respectively. Glycopeptide peaks from the spiked injections could be clearly observed in the mass spectra after enrichment and verified the applicability for TCMIs injection. In summary, after the enrichment of the three glycoprotein-spiked TCMIs using mMOF–AAPBA, it is evident that all the enriched glycopeptides are originated from the spiked HRP. These results reminds that the three injections may not contain glycopeptide components. The glycopeptide peak information of the three spiked traditional Chinese medicine injections is shown in Table S7.

4. Conclusions

In conclusion, a boronic acid-functionalized magnetic zirconium metal-organic framework (mMOF–AAPBA) with PDA as the intermediary was synthesized and applied in the MSPE separation and enrichment of glycopeptides. The most interesting aspect of this study is that,

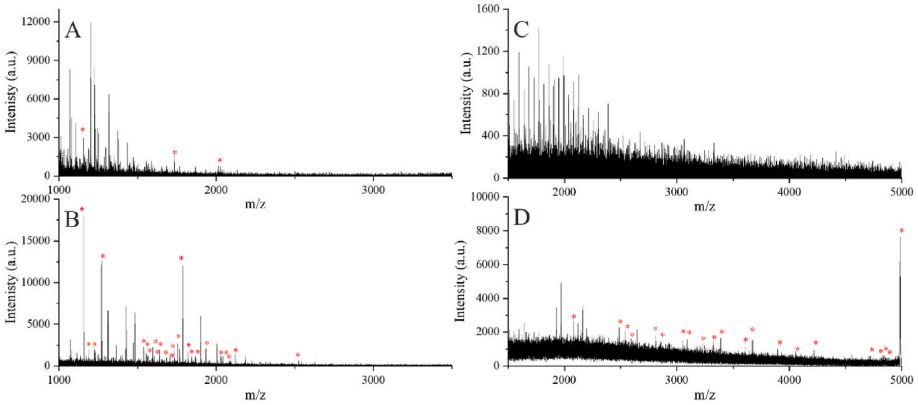

Fig. 8. MALDI-TOF mass spectra of human saliva before (A) and after (B) enrichment with mMOF–AAPBA and HRP-spiked SM injection tryptic digests before (C) and after (D) enrichment with mMOF–AAPBA. Peaks of glycopeptides are labeled with "*".

during the characterization process, a protocol for accurate determination of boron in MOFs based nanocomposites was developed by using LA-ICP-MS in combination with ICP-OES, and being validated with home-made MRMs. The acquisition of actual boron content may not only facilitate the prospective design of novel boronate affinity materials, but also deepen the understanding to the interaction mechanisms towards *cis*-diols-containing analytes including glycopeptides. Another one is that the nanocomposite prepared with PDA as bridge for post-modification of UiO-66–NH_2 and then boronic acid, which aligns with the principles of green chemistry, captured glycopeptides through the synergistic effect of HILIC and BAC mechanisms. In addition, it is well known that post-synthetic modification allows higher utilization efficiency and exposing rate of boronic acid groups. This is probably the cause the excellent performance in enriching glycopeptides of mMOF–AAPBA was observed in IgG and HRP digests. Furthermore, human saliva and TCMIs were employed as real-world samples for assessing the applicability of the boronate affinity material for glycopeptides, which indicated that mMOF–AAPBA is a promising candidate for capturing *cis*-diols compounds from multiple kinds of biological samples.

CRediT authorship contribution statement

Feng Zhang: Writing – original draft, Visualization, Methodology, Formal analysis. **Sen Zhang:** Writing – original draft, Visualization, Investigation, Data curation. **Xing Liu:** Resources, Methodology, Formal analysis. **Wei Gao:** Methodology, Investigation. **Jun Luo:** Resources, Methodology. **Yi-fan Pan:** Methodology, Investigation. **Wei-Juan Zheng:** Methodology, Funding acquisition. **Xin Hu:** Resources. **Hongzhen Lian:** Writing – review & editing, Supervision, Project administration, Funding acquisition, Conceptualization.

Declaration of competing interest

The authors declare that they have no known competing financial interests or personal relationships that could have appeared to influence the work reported in this paper.

Acknowledgements

This work was supported by the National Key R&D Program of China (No. 2024YFF0618100), and the National Natural Science Foundation of China (22176085 and 21874065).

Appendix A. Supplementary data

Supplementary data to this article can be found online at https://doi.org/10.1016/j.aca.2025.344511.

Data availability

Data will be made available on request.

References

[1] N. Haines, K.D. Irvine, Glycosylation regulates notch signalling, Nat. Rev. Mol. Cell Biol. 4 (2003) 786–797, https://doi.org/10.1038/nrm1228.
[2] M. Fournet, F. Bonté, A. Desmoulière, Glycation damage: a possible hub for major pathophysiological disorders and aging, Aging Dis. 9 (2018) 880–900, https://doi.org/10.14336/AD.2017.1121.
[3] W. Morelle, K. Canis, F. Chirat, V. Faid, J.C. Michalski, The use of mass spectrometry for the proteomic analysis of glycosylation, Proteomics 6 (2006) 3993–4015, https://doi.org/10.1002/pmic.200600129.
[4] B. Mann, M. Madera, I. Klouckova, Y. Mechref, L.E. Dobrolecki, R.J. Hickey, Z. T. Hammound, M.V. Novotny, A quantitative investigation of fucosylated serum glycoproteins with application to esophageal adenocarcinoma, Electrophoresis 31 (2010) 1833–1841, https://doi.org/10.1002/elps.201000046.
[5] J. Wohlgemuth, M. Karas, T. Eichhorn, R. Hendriks, S. Andrecht, Quantitative site-specific analysis of protein glycosylation by LC-MS using different glycopeptide-enrichment strategies, Anal. Biochem. 395 (2009) 178–188, https://doi.org/10.1016/j.ab.2009.08.023.
[6] H. Geyer, R. Geyer, Strategies for analysis of glycoprotein glycosylation, Biochim. Biophys. Acta 1764 (2006) 1853–1869, https://doi.org/10.1016/j.bbapap.2006.10.007.
[7] H.Y. Zhang, G.P. Yao, C.H. Deng, H.J. Lu, P.Y. Yang, Facile synthesis of boronic acid-functionalized magnetic mesoporous silica nanocomposites for highly specific enrichment of glycopeptides, Chin. J. Chem. 29 (2011) 835–839, https://doi.org/10.1002/cjoc.201190166.
[8] Z.H. Hu, W.Q. Gao, R. Liu, J.Q. Yang, R.L. Han, J.H. Li, J.C. Yu, D.H. Ma, K. Q. Tang, An efficient strategy with a synergistic effect of hydrophilic and electrostatic interactions for simultaneous enrichment of N- and O-glycopeptides, Analyst 149 (2023) 1090–1101, https://doi.org/10.1039/d3an01888a.
[9] S.Y. Kong, Q.Q. Zhang, L.J. Yang, Y.Y. Huang, M.Q. Liu, G.Q. Yan, H.H. Zhao, M. X. Wu, X.M. Zhang, P.Y. Yang, W.Q. Cao, Effective enrichment strategy using boronic acid-functionalized mesoporous graphene-silica composites for intact N- and O-linked glycopeptide analysis in human serum, Anal. Chem. 93 (2021) 6682–6691, https://doi.org/10.1021/acs.analchem.0c05482.
[10] D. Chettri, M. Boro, L. Sarkar, A.K. Verma, Lectins: biological significance to biotechnological application, Carbohydr. Res. 506 (2021) 108367, https://doi.org/10.1016/j.carres.2021.108367.
[11] H.H. Bai, Y.T. Pan, L. Qi, L. Liu, X.Y. Zhao, H.Y. Dong, X.Q. Cheng, W.J. Qin, X. H. Wang, Development a hydrazide-functionalized thermosensitive polymer based homogeneous system for highly efficient N-glycoprotein/glycopeptide enrichment from human plasma exosome, Talanta 186 (2018) 513–520, https://doi.org/10.1016/j.talanta.2018.04.098.
[12] Y.Y. Yan, R.L. Han, Y.F. Hou, H.J. Zhang, J.C. Yu, W.Q. Gao, L. Xu, K.Q. Tang, Bowl-like mesoporous polydopamine with size exclusion for highly selective recognition of endogenous glycopeptides, Talanta 233 (2021) 122468, https://doi.org/10.1016/j.talanta.2021.122468.
[13] Z.Y. Li, Y.C. Gao, P. An, F. Lan, Y. Wu, Hydrophilic magnetic covalent organic frameworks for highly integrated pre-enrichment and analysis of colorectal cancer differential glycoproteomics, Mater. Des. 217 (2022) 110584, https://doi.org/10.1016/j.matdes.2022.110584.
[14] B. Luo, G.H. Li, Z.Y. Li, J. He, J. Zhou, L.J. Wu, F. Lan, Y. Wu, Construction of a magnetic covalent organic framework with synergistic affinity strategy for enhanced glycopeptide enrichment, J. Mater. Chem. B 9 (2021) 6377–6386, https://doi.org/10.1039/d1tb01168e.

[15] Y.X. Wang, W.H. Xu, H. Xu, Q. Jia, Preparation of tannic acid and L-cysteine functionalized magnetic composites for synergistic enrichment of N-glycopeptides followed by mass spectrometric analysis, Anal. Methods 14 (2022) 3260–3269, https://doi.org/10.1039/d2ay01169g.
[16] P. Su, M. Li, X. Li, X.Y. Yuan, Z. Gong, L.Q. Wu, J.Y. Song, Y. Yang, Glutathione functionalized magnetic covalent organic frameworks with dual-hydrophilicity for highly efficient and selective enrichment of glycopeptides, J. Chromatogr. A 1667 (2022) 462869, https://doi.org/10.1016/j.chroma.2022.462869.
[17] W. Gao, F. Zhang, S. Zhang, J.Y. Li, H.Z. Lian, Hydrophilic porous magnetic graphene oxide/chitosan composites for the selective separation and enrichment of N-glyco- and phosphopeptides, ACS Appl. Nano Mater. 6 (2023) 15563–15573, https://doi.org/10.1021/acsanm.3c02350.
[18] P. Su, Z. Wang, X. Li, M. Li, G. Li, Z. Gong, J.Y. Song, Y. Yang, Fabrication of magnetic dual-hydrophilic metal organic framework for highly efficient glycopeptide enrichment, Anal. Bioanal. Chem. 413 (2021) 5267–5278, https://doi.org/10.1007/s00216-021-03535-w.
[19] X.T. Jin, C.H. Zhu, J.N. Wu, Y.H. Yan, C.F. Ding, K.Q. Tang, D. Zhang, Hydrophilic carrageenan functionalized magnetic carbon-based framework linked by silane coupling agent for the enrichment of N-glycopeptides from human saliva, J. Separ. Sci. 44 (2021) 2143–2152, https://doi.org/10.1002/jssc.202001216.
[20] H.Z. Jin, W.Q. Gao, R. Liu, J.Q. Yang, S. Zhang, R.L. Han, J. Lin, S.J. Zhang, J. C. Yu, K.Q. Tang, A novel hydrophilic hydrogel with a 3D network structure for the highly efficient enrichment of N-glycopeptides, Analyst 147 (2022) 2425–2432, https://doi.org/10.1039/d2an00516f.
[21] M. Wu, Q. Zhang, Q.Y. Zhang, H. Wang, F.W. Wang, J.M. Liu, L.Q. Guo, K. Song, Research progress of UiO-66-based electrochemical biosensors, Front. Chem. 10 (2022) 842894, https://doi.org/10.3389/fchem.2022.842894.
[22] K. Chattopadhyay, M. Mandal, D.K. Maiti, A review on zirconium-based metal-organic frameworks: synthetic approaches and biomedical applications, Mater. Adv. 5 (2024) 51–67, https://doi.org/10.1039/d3ma00735a.
[23] D.J. Li, Y. Chen, Z. Liu, Boronate affinity materials for separation and molecular recognition: structure, properties and applications, Chem. Soc. Rev. 44 (2015) 8097–8123, https://doi.org/10.1039/c5cs00013k.
[24] B.C. Wang, J.M. Liu, Y.H. Yan, C.F. Ding, K.Q. Tang, Post-synthesis of boric acid-functionalized magnetic covalent organic framework as an affinity probe for the enrichment of N-glycopeptides, Microchim. Acta 188 (2021) 336, https://doi.org/10.1007/s00604-021-04998-5.
[25] C. Zhang, X.D. Jin, L.P. Wang, L.P. Wang, C.Z. Jin, X.Q. Han, W.G. Ma, X.G. Li, G. X. Teng, Hollow $MnFe_2O_4$@C@APBA nanospheres with size exclusion and pH response for efficient enrichment of endogenous glycopeptides, ACS Appl. Mater. Interfaces 13 (2021) 9714–9728, https://doi.org/10.1021/acsami.0c22221.
[26] S.C. Liu, Z. Hu, X. Zhang, N.A. Tang, H.X. Ou, J.M. Pan, Selective separation of target glycoproteins using boronate affinity imprinted copolymers: precise identification and increase the number of recognition sites, Sep. Purif. Technol. 326 (2023) 124865, https://doi.org/10.1016/j.seppur.2023.124865.
[27] L.T. Liu, Y. Zhang, L. Zhang, G.Q. Yan, J. Yao, P.Y. Yang, H.J. Lu, Highly specific revelation of rat serum glycopeptidome by boronic acid-functionalized mesoporous silica, Anal. Chim. Acta 753 (2012) 64–72, https://doi.org/10.1016/j.aca.2012.10.002.
[28] Y. Wang, X. Zhang, Z.H. Wei, Y.J. Jiao, D.Y. An, Y.P. Huang, Z.S. Liu, C. Yan, Dual-function monolithic enzyme reactor based on dopamine/graphene oxide coating for simultaneous protein enzymatic hydrolysis and glycopeptide enrichment, J. Chromatogr. A 1666 (2022) 462848, https://doi.org/10.1016/j.chroma.2022.462848.
[29] A. Kenji, I. Hiroki, K. Hiroyuki, H. Yasui, Strong binding affinity of D-allulose and allulosides to boronic acids and the structural characterization of their sugar-boronate complexes, Chem. Lett. 50 (2021) 1470–1474, https://doi.org/10.1246/cl.210181.
[30] D.J. Li, S.H. Dong, 6-Aminopyridine-3-boronic acid functionalized magnetic nanoparticles for highly efficient enrichment of *cis*-diol-containing biomolecules, Anal. Methods 13 (2021) 2331–2337, https://doi.org/10.1039/d1ay00414j.
[31] W.G. Roshan, Y. Zhao, Recognition and protection of glycosphingolipids by synthetic nanoparticle receptors, Chem. Commun. 55 (2019) 4773–4776, https://doi.org/10.1039/c9cc01694e.
[32] F.F. Xiong, T. Zhang, J.T. Ma, Q. Jia, Dual-ligand hydrogen-bonded organic framework: tailored for mono-phosphopeptides and glycopeptides analysis, Talanta 266 (2024) 125068, https://doi.org/10.1016/j.talanta.2023.125068.
[33] C.H. Lu, H.D. Wei, L.Z. Xu, W.L. Wang, C. Yang, X.L. Shi, H. Gao, Y.W. Feng, J. Z. Zhou, Y. Zhang, Enrichment of sialic acid-containing casein glycomacropeptide in protein hydrolysates using phenylboronic acid-functionalized mesoporous silica nanoparticles, Talanta 267 (2024) 125174, https://doi.org/10.1016/j.talanta.2023.125174.
[34] S.C. Liu, Y. Sun, D.Z. Guo, Y.Y. Mao, B. Bai, Z.J. Li, Emulsion interfacial synthesis of hierarchically porous covalent organic framework microcapsules with multilayered boronic acid binding sites for specific molecular separation, Appl. Surf. Sci. 635 (2023) 157695, https://doi.org/10.1016/j.apsusc.2023.157695.
[35] Z.H. Zhao, Y.J. Huang, W.R. Liu, F.G. Ye, S.L. Zhao, Immobilized glucose oxidase on boronic acid-functionalized hierarchically porous mof as an integrated nanozyme for one-step glucose detection, ACS Sustainable Chem. Eng. 8 (2020) 4481–4488, https://doi.org/10.1021/acssuschemeng.9b07631.
[36] Y.D. Xu, Y. Sun, Z.W. Yao, Y.M. Wei, Hierarchical mesoporous metal-organic frameworks with boric acid sites on the inner surface of small mesopores for the extraction of nucleotides in human plasma samples, ACS Appl. Mater. Interfaces 15 (2023) 30643–30652, https://doi.org/10.1021/acsami.3c05025.
[37] W. Gao, F. Zhang, S. Zhang, J.Y. Li, H.Z. Lian, Ti(IV) immobilized bisphosphate fructose-modified magnetic Zr metal organic framework (MOF) for specific enrichment of phosphopeptides, Sep. Purif. Technol. 305 (2023) 122426, https://doi.org/10.1016/j.seppur.2022.122426.
[38] H.A. Hamzah, T.S. Crickmore, D. Rixson, A.D. Burrows, Post-synthetic modification of zirconium metal-organic frameworks by catalyst-free aza-Michael additions, Dalton Trans. 47 (2018) 14491–14496, https://doi.org/10.1039/c8dt03312a.
[39] D.X. Yin, W. Fang, D.X. Guan, P.N. Williams, E. Moreno-Jimenez, Y. Gao, F.J. Zhao, L.Q. Ma, H. Zhang, J. Luo, Localized intensification of arsenic release within the emergent rice rhizosphere, Environ. Sci. Technol. 54 (2020) 3138–3147, https://doi.org/10.1021/acs.est.9b04819.
[40] F.A. Stevie, C.L. Donley, Introduction to x-ray photoelectron spectroscopy, J. Vac. Sci. Technol. A 38 (2020) 063204, https://doi.org/10.1116/6.0000412.
[41] N. Stojilovic, Why can't we see hydrogen in X-ray photoelectron spectroscopy, J. Chem. Educ. 89 (2012) 1331–1332, https://doi.org/10.1021/ed300057j.
[42] X.Y. Long, J.Y. Li, D. Sheng, H.Z. Lian, Low-cost iron oxide magnetic nanoclusters affinity probe for the enrichment of endogenous phosphopeptides in human saliva, RSC Adv. 6 (2016) 96210–96222, https://doi.org/10.1039/c6ra11125d.
[43] J.Y. Li, S. Zhang, W. Gao, Y. Hua, H.Z. Lian, Guanidyl-functionalized magnetic bimetallic MOF nanocomposites developed for selective enrichment of phosphopeptides, ACS Sustain. Chem. Eng. 8 (2020) 16422–16429, https://doi.org/10.1021/acssuschemeng.0c04118.
[44] B.F. Zhao, Y.X. Wang, J.T. Ma, Q. Jia, Design of a hydrophilic mercaptosuccinic acid-functionalized beta-cyclodextrin polymer *via* host-guest interaction: toward highly efficient glycopeptide enrichment, Analyst 147 (2022) 4553–4561, https://doi.org/10.1039/d2an01358d.
[45] D.H. Xu, C.L. Yu, J.J. Wang, Q.R. Fan, Z.Z. Wang, W. Xiao, J.A. Duan, J. Zhou, H. Y. Ma, Ultrafiltration strategy combined with NanoLC-MS/MS based proteomics for monitoring potential residual proteins in TCMIs, J. Chromatogr. B 1178 (2021) 122818, https://doi.org/10.1016/j.jchromb.2021.122818.
[46] S. Zhang, J.Y. Li, W. Gao, J.Q. Qiao, H.Z. Lian, Magnetic Ti_3C_2 MXene nanosheets prepared for enrichment of phosphopeptides, ACS Appl. Mater. Interfaces 15 (2023) 16505–16514, https://doi.org/10.1021/acsami.3c00848.